Storminess Variability along the California Coast: 1858–2000

PETER D. BROMIRSKI

Integrative Oceanography Division, Scripps Institution of Oceanography, University of California, San Diego, La Jolla, California

REINHARD E. FLICK

California Department of Boating and Waterways, Integrative Oceanography Division, Scripps Institution of Oceanography, University of California, San Diego, La Jolla, California

DANIEL R. CAYAN

Climate Research Division, Scripps Institution of Oceanography, University of California, San Diego, and U.S. Geological Survey, La Jolla, California

(Manuscript received 4 February 2002, in final form 5 August 2002)

ABSTRACT

The longest available hourly tide gauge record along the West Coast (U.S.) at San Francisco yields meteorologically forced nontide residuals (NTR), providing an estimate of the variation in ''storminess'' from 1858 to 2000. Mean monthly positive NTR (associated with low sea level pressure) show no substantial change along the central California coast since 1858 or over the last 50 years. However, in contrast, the highest 2% of extreme winter NTR levels exhibit a significant increasing trend since about 1950. Extreme winter NTR also show pronounced quasi-periodic decadal-scale variability that is relatively consistent over the last 140 years. Atmospheric sea level pressure anomalies (associated with years having high winter NTR) take the form of a distinct, large-scale atmospheric circulation pattern, with intense storminess associated with a broad, southeasterly displaced, deep Aleutian low that directs storm tracks toward the California coast.

1. Introduction

Increased coastal erosion and flooding from intense storm activity along the California coast occurred during the great El Niños of 1982/83 and 1997/98. How does this level of ''storminess'' compare with other strong El Niños over the past century? Has storminess increased along the West Coast? Knowing whether storminess is increasing is important for coastal planning and establishing design criteria for future coastal development, as well as being an indicator of potential anthropogenically forced or naturally occurring climate change.

Meteorologically forced storminess is associated with propagating low pressure systems (cyclones) that can be characterized by various aspects of sea level pressure (SLP), wind speed, and resulting synoptic changes in sea level. In the extratropical North Pacific, most storminess is associated with winter cyclones, usually characterized by low surface pressure with high winds and precipitation. Over the ocean, cyclones cause episodic increases in ocean surface gravity wave energy and elevate sea levels. Over land, the primary indicator of storminess is accumulated precipitation that can be strongly influenced by topography and related orographic effects. Because of spatial variation and because estimates of storminess using these parameters are dependent on both their intensity and duration, each of these measures of storminess has somewhat different temporal and amplitude characteristics.

An increasing trend in the number and intensity of midlatitude cyclones in the central North Pacific in the last 50 yr has been identified (Graham and Diaz 2001), although the tracking domain did not include the region within 5° of the West Coast (U.S.). Because cyclones tend to turn northward as they mature and to decay as they move eastward (Anderson and Gyakum 1989), the impact of increased cyclone activity in the central North Pacific on the West Coast depends on a storm's behavior in the extreme eastern Pacific, which may differ substantially from its open-ocean characteristics. Hindcasts of significant wave height (H_s) using National Centers for Environmental Prediction–National Center for Atmospheric Research (NCEP–NCAR) reanalysis wind fields also show increasing trends of extreme H_s over

Corresponding author address: Dr. Peter D. Bromirski, Integrative Oceanography Division, Scripps Institution of Oceanography, 8602 La Jolla Shores Dr., La Jolla, CA 92037.
E-mail: pbromirski@ucsd.edu

the past 40 yr (Wang and Swail 2001; Graham and Diaz 2001), presumably associated with increased cyclone intensity. However, because model-derived hindcasts do not model short-period wave energy reliably, the magnitude of wave and associated storm activity at coastal locations from such hindcasts can be uncertain. Thus, measures of storminess at or near the West Coast are invaluable for gaging the coastal vulnerability to climate variability.

As an alternative to uncertainties associated with both model-generated hindcasts and near-coastal storm behavior, the long-term variability of storminess along the California coast can be estimated from nearly continuous hourly tide gauge data from San Francisco (SFO) that span the 1858–2000 time period. The location of San Francisco on the California coast (37.8°N, 122.6°W) is sensitive to changes in both the intensity and tracks of North Pacific winter storms. Because nontidal sea level fluctuations are forced largely by SLP and wind, and are reasonably well correlated with short-period gravity waves as well as precipitation, meteorologically forced water level variation gives a useful composite estimate of storminess. The SFO hourly tide gauge record is unique in North America in both its length and continuity, and thus provides an unbiased climate-related time series of sufficient duration to investigate interdecadal storminess (climate) variability along the West Coast. Also, the hourly sampling rate allows better characterization of synoptic events than more coarsely sampled pre-1948 SLP and precipitation data, which are generally available only at daily resolution.

Climate variability in the North Pacific driven by El Niño–forced teleconnections from the Tropics has been the subject of numerous studies (cf. Bjerknes 1969; Latif et al. 1998). North Pacific climate variability on decadal timescales and longer is estimated from datasets, usually augmented by objective analysis, of at most 100-yr duration (e.g., Trenberth and Hurrell 1994; Mantua et al. 1997; Graham and Diaz 2001). Hence, most estimates of interdecadal climate variability are based on oceanic and meteorologic data that span few cycles (assuming periodicity). Because central California coastal climate variability is affected by Pacific basin–scale phenomena, the SFO tide gauge record that spans 140 years can provide an independent estimate of relatively long-term climate variability in the eastern North Pacific.

2. Data sources

Hourly tide gauge data from SFO were obtained from the National Oceanic and Atmospheric Administration (NOAA) National Ocean Service (NOS) Center for Operational Oceanographic Products and Services (CO-OPS). The tide gauge data were collected at three locations east of the Golden Gate Bridge: Fort Point (June 1854–November 1877), Sausalito (February 1877–September 1897), and The Presidio (July 1897–present; Fig. 1). Leveling to established benchmarks from San Francisco to Sausalito shows no elevation change at Sausalito from 1877 to 1977 (Smith 1980), indicating that the tide gauge stations are referred to a common reference datum and that relative gauge height comparisons are consistent. Data prior to May 1858 have unexplained trends and datum shifts and are therefore not considered.

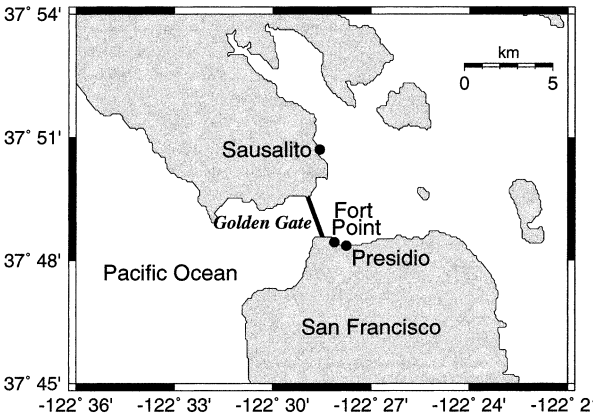

FIG. 1. Locations of the San Francisco tide gauge at Fort Point, Sausalito, and The Presidio, San Francisco (Smith 1980), just inside the Golden Gate Bridge.

Other data used in this study include hourly SLP and wind speed (Ws) data from the San Francisco International Airport (1948–2000), obtained from the NOAA National Climatic Data Center (NCDC). Monthly precipitation data collected at San Francisco were obtained from Sus Tabata, Institute of Ocean Science, Sidney, BC, Canada (1850–1950); the Department of Water Resources, California (1951–88); and the Western Regional Climate Center, Reno, Nevada (1989–2000). Wave spectral density estimates used to determine hourly short-period wave height estimates were obtained for buoy 46026 (1982–2000) from the NOAA National Data Buoy Center (NDBC). Buoy 46026 is located about 20 km west of the Golden Gate Bridge at (37.759°N, 122.833°W).

3. Nontide water levels

Tide gauge water levels are dominated by astronomically forced ocean tides (high-amplitude blue spectral lines in Fig. 2), but also include internal wave energy and overtides that are generated over relatively local topography (Munk and Cartwright 1966) as well as meteorologically forced components (Flick 1986). Other factors affecting water levels include steric, wind-forced, and atmospheric pressure changes associated with seasonal variation and anomalous climatic variations such as El Niño (Reid and Mantyla 1976). The astronomical tidal constituents vary slightly over time (Cartwright 1972), and the amount of internal wave energy found within the tidal species is difficult to estimate. The need for estimating these factors over the 140-yr SFO data record was eliminated by implement-

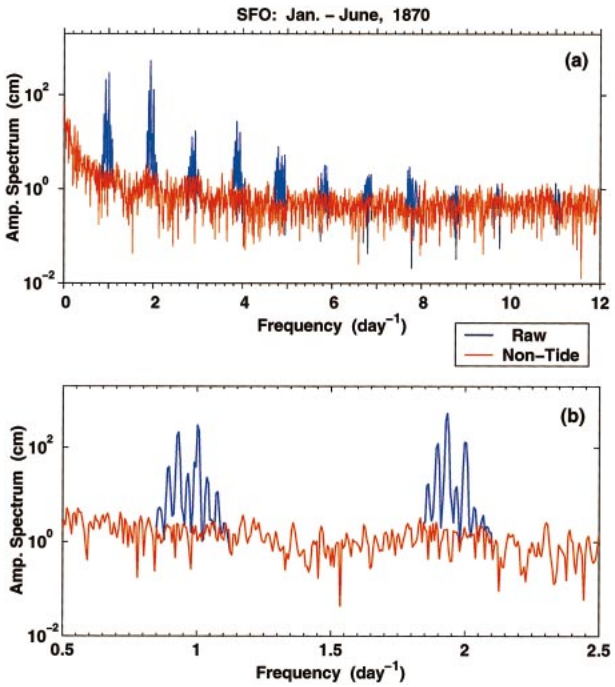

FIG. 2. (a) Representative tide gauge spectrum (blue) with the associated nontide spectrum (red) obtained from a 4096-h data segment at the beginning of 1870. (b) Expanded view of the first two tidal species showing that the nontide filtering methodology produces spectral estimates virtually indistinguishable from the continuum.

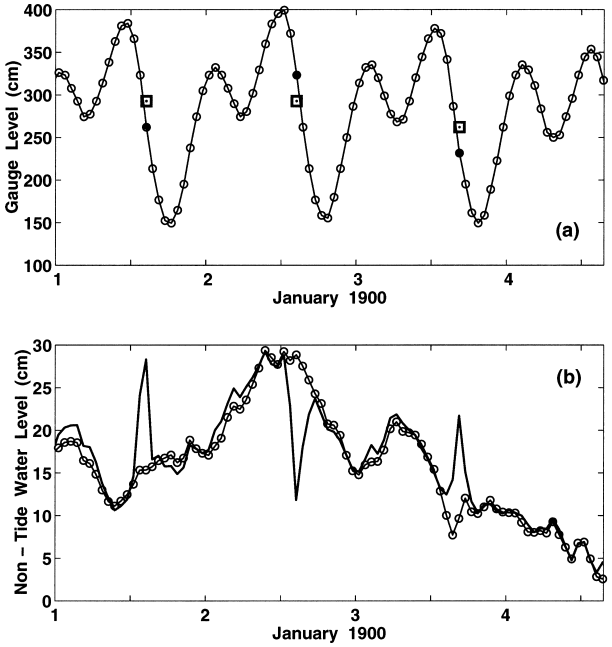

FIG. 3. (a) Raw tide gauge data for 1–4 Jan 1900. Circles indicate actual measurements. Filled circles indicate measurements that were shifted to the levels of the adjacent dots enclosed by squares. (b) Nontide water levels (thin line with circles) determined for the raw, unmodified tide gauge data in (a), and corresponding nontide water level estimates obtained for the same data but substituting data points at the squares for the filled circles (thick solid line).

ing a spectral method of tide constituent removal that preserves estimates of the meteorologically forced components across the tidal species.

Assuming that the continuum of nontidal forcing varies smoothly across the tidal species, nontide water levels are obtained with frequency domain operations that estimate continuum spectral levels within the tide bands. Sequential 4096-h data blocks were transformed to the frequency domain by fast Fourier transform (FFT) after applying a Hanning window to the demeaned, detrended data segment, giving the amplitude spectrum in Fig. 2 (blue lines). Using data blocks of this length effectively acts as a high-pass filter with about a 6-month period. The range of variability of both the real and imaginary parts of the resulting spectrum were estimated for the 10 spectral estimates below each tide band, about 25% of the number of spectral estimates in each tide band for the bandwidth used (see Pugh 1987 for tide band frequencies). The variance estimate for each tide band was multiplied by n random numbers in the $(-1, 1)$ range, where n is the number of spectral estimates in each respective tide band. The trends of the real and imaginary components across the tide bands were estimated. The randomized variance estimates were then added to respective trend-derived amplitude estimates of the real and imaginary parts for each spectral estimate in each tide band. This filtering methodology provides both amplitude and phase estimates across the tidal species that are consistent with those of the concurrent nontide continuum. The resulting nontide amplitude spectrum across the tidal species (Fig. 2, red lines) is essentially indistinguishable from unmodified spectral estimates on either side of the tide bands. Inverse FFT of the modified tide gauge spectrum to the time domain with window correction gives the nontide water level estimate, followed by application of a three-point triangular filter to suppress high-frequency processing artifacts.

The stability of the phase of the nontide water levels can be demonstrated by comparing the nontide levels before and after introducing ''glitches'' in the raw data. Figure 3a shows a portion of SFO tide gauge data from January 1900, with circles showing actual data amplitudes. The corresponding nontide levels are shown in Fig. 3b (thin line with circles). The data points having solid circles in Fig. 3a were replaced with those in the squares [a shift of 30.5 cm (1 ft) in the tide gauge data]. The resulting nontide amplitudes differ markedly from the unmodified nontide levels near the glitch points, with small differences at other points resulting from related changes in the Fourier coefficients. Note that the associated spikes have the same sign and occur at about the same time as the point shifts, indicating that this filtering methodology produces little if any phase distortion. Such spikes in actual nontide data were used to identify glitches in the raw tide gauge data resulting

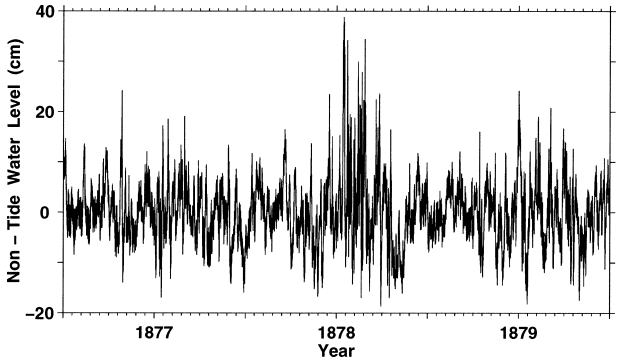

FIG. 4. Nontide water levels encompassing the time period before and after the change in the tide gauge data source location in Nov 1877 from Fort Point to Sausalito (see Fig. 1).

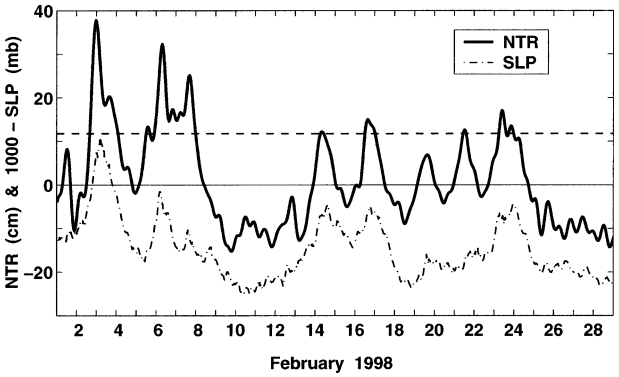

FIG. 5. NTR (thick line) and SLP (dot–dashed line) at SFO during Feb 1998, a month during El Niño with exceptionally high storm activity. Note that 1000 − SLP is plotted, so SLP > 0 corresponds to SLP less than 1000 mb, that is, an intense storm. The 98th percentile from the ranking of all hourly NTR from 1858–2000 (horizontal dashed line, NTR = 11.46) indicates the NTR level used to produce Figs. 7b and 7c.

from transcription and data entry errors, with hundreds of corrections necessary in the recently available pre-1900 data. Assuming that nontide continuum amplitudes vary relatively smoothly in time (Munk and Cartwright 1966), glitch points identified were interactively adjusted until the nontide amplitudes in the vicinity of the glitch points had the same general trend and character as nearby nontide levels. This correction methodology has the advantage of needing no external datasets, for example, predicted tide or SLP, to make necessary adjustments that are consistent with current continuum characteristics.

The nontide spectrum (Fig. 2a, red line) provides an estimate of meteorologically forced water levels. Successive 4096-h data blocks were processed with a 50% overlap, with the exterior half of the overlapping data discarded to avoid window edge effects. Inspection of resulting nontide water level data showed no discontinuities or variability that could be related to the processing methodology. This is demonstrated in Fig. 4 for nontide data that spans the change in the tide gauge location in November 1877 from Fort Point on the south side of San Francisco Bay to the north side at Sausalito (see Fig. 1). Although high-amplitude nontide water levels are observed during winter months, especially during the very strong 1877/78 El Niño event (Quinn and Neal 1987), no discernible variation is observed that can be attributed to the processing methodology. Indeed, because the tide response is most likely quite different at Sausalito than at San Francisco, this suggests that this filtering methodology can be applied to common datum-referenced tide gauge data where appreciable changes in local bathymetry or shorelines over time have affected the local tidal response.

Nontide residual (NTR) water levels are obtained from the nontide data by bandpass [(1/30, 2.5) day^{-1}] filtering both forward and reverse (ensuring no phase distortion) using a low-pass Chebyshev type-I filter of order 10 and a high-pass elliptical filter of order 6 (Krauss et al. 1995), chosen for the necessary steep cutoff of the low-frequency energy. Although this filter combination has sharp cutoffs, no evidence of ''ringing'' is observed in the time domain (see Fig. 5). This passband excludes steric and other sea level variation at timescales longer than 30 days and short-period variation resulting from overtides and minor data irregularities. These cutoffs were chosen to give sufficient temporal resolution to accurately study NTR changes on synoptic timescales.

NTR estimates obtained with the above methodology include variability not related to meteorological forcing. These variations result from both the inclusion of some tidal ''cusp'' energy that results from nonlinear interactions between the tidal constituents and the lowest continuum frequencies (Munk and Cartwright 1966) and the statistical variability associated with the randomly generated spectral estimates across the tidal species. To estimate the importance of these factors, 10 NTR realizations were computed for the entire tide gauge record with the tide bands extended about 30%, that is, 15% on both sides of each band, thus excluding most cusp frequencies. The 98th percentile level was determined from the ranking of all NTR data for each realization in order to estimate the impact of NTR variability on extreme storminess analyses. The means (μ) and standard deviations (σ) were determined for the 10 realizations of the 98th percentile levels and the associated maximum and minimum NTR values for each realization, giving (98th: $\mu = 11.3837$, $\sigma = 0.0037$) cm, (max.: $\mu = 45.1836$, $\sigma = 0.0899$) cm, and (min.: $\mu = -28.0783$, $\sigma = 0.2569$) cm, respectively. These values show very small variability and differ from those of the narrower tide band NTR estimates in Fig. 2 by less than 1%, suggesting that the NTR do not include substantial cusp energy and that tidal species band-limit selection is not critical. Thus, the small variability associated with the filtering methodology should not affect general con-

clusions about storminess deduced from NTR variations.

4. Meteorologically forced sea level changes

Variation in sea level pressure (SLP) causes an ''inverse barometer'' effect on tide gauge water levels, with water levels tending to rise under low SLP and be depressed under high SLP (Chelton and Davis 1982). Because the water level response to meteorological events depends on the location of the center of the low relative to the tide gauge, the SLP gradient (and associated wind speed and direction), and the rate of storm movement, meteorologically forced water level fluctuations at coastal locations can include a nonlocal component that reduces the correlation with SLP. Also, alongshore winds south of the tide gauge can generate coastally trapped waves that propagate northward and elevate water levels (Enfield and Allen 1980). These nonlocal factors, and presumably also the effects of local winds, appear to reinforce the local inverse barometer effect on San Francisco sea level anomalies. As seen in Fig. 6a, the ratio of NTR to (1/30, 2.5) day^{-1} bandpass-filtered SLP is about 1.65 cm mb^{-1}, substantially larger than the commonly accepted inverse barometric response of 1 cm mb^{-1}. Thus, NTR variation provides a local-to-regional-scale measure of storminess. The importance of the regional component on NTR is demonstrated in Fig. 5 where the variation in NTR (thick line) follows the variation in SLP (dot–dashed line), but the relative amplitudes of the peaks do not always correspond. However, in general, low SLP (i.e., intense storminess) corresponds to high nontide residuals.

After comparing several measures of NTR with other measures of storminess (not available for as long a time period), it became apparent that the cumulative NTR anomaly, calculated as the sum of the hourly NTR $>$ 0 (NTRp) within a month and normalized by the number of hourly measurements in that month, gives a reasonable estimate of storminess. Other measures of storminess, such as variation in either SLP, wind speed (Ws), or short-period significant wave height (SP H_s, waves having periods less than 8 s that are dominated by regional wind stress characteristics) are also subject to ambiguities related to the SLP gradient and storm propagation parameters, and SP H_s can also include a significant nonlocal component. For these reasons, correlations of cumulative hourly SLP, SP H_s, and Ws anomalies with NTRp for winter months (December–March) show substantial scatter (Figs. 6a–c). Comparisons for entire winter periods were made because there is substantial year-to-year variability for the individual months. Hourly SLP, Ws, and SP H_s anomalies were obtained from differences with their respective seasonal means, followed by application of the same (1/30, 2.5) day^{-1} bandpass filter used to obtain the hourly NTR. Anomalies of SP H_s were determined for all available hourly wave spectra from NOAA buoy 46026.

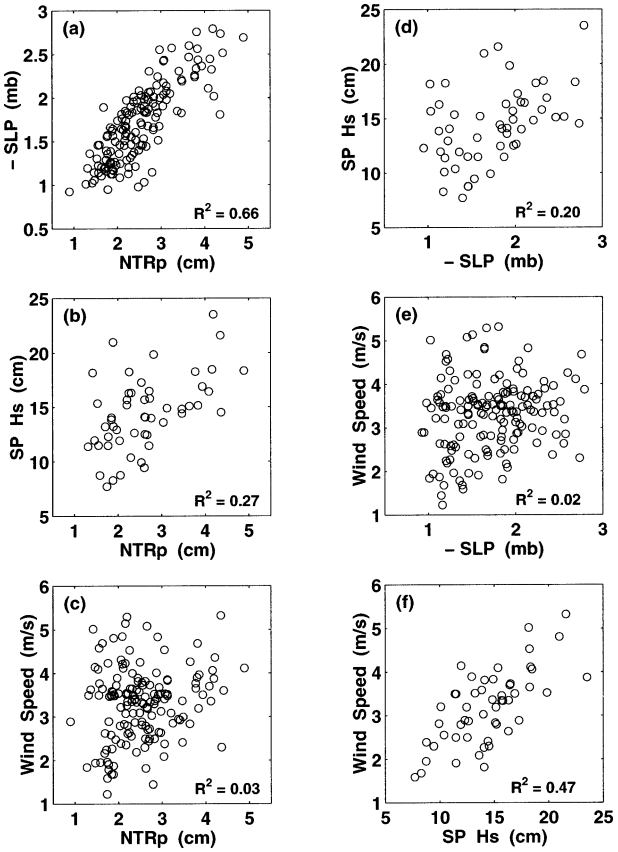

FIG. 6. Cumulative winter anomalies of (a) SLP, (b) SP H_s, and (c) Ws vs winter NTRp, with associated R^2 indicated. (d), (e), (f) Correlations between the non-NTR parameters. NTRp, SLP, and Ws span the 1948–99 time period, while SP H_s from wave spectral estimates at NOAA buoy 46026 are available from 1982 onward. Plotted for winter months (Dec–Mar) are sums of SLP $<$ 0, Ws $>$ 0, and SP $H_s > 0$ hourly anomalies and NTR $>$ 0, each normalized by the number of available measurements in each winter.

The relatively high correlation ($R^2 = 0.66$) observed between winter NTRp and negative SLP anomalies (Fig. 6a) indicates a close relationship between low SLP (storminess) and high NTRp during winter months. Correlation of SLP with SP H_s (Fig. 6d) has similar scatter to that of NTRp versus SP H_s (Fig. 6b), consistent with the observed relationship between NTRp and SLP. Regional relatively high SLP can result in strong SLP gradients that generate strong winds not associated with storminess. Consequently, correlation between anomalies of Ws and SLP is poor on winter timescales (Fig. 6e), and is consistent with the low correlation observed between Ws and NTRp (Fig. 6c) and the marginal correlation observed between sea level anomalies and alongshore wind stress in the San Francisco region (Enfield and Allen 1980). Thus, strong winds are not necessarily the best measure of intense regional storms, but are likely to generate short-period waves as is evidenced by the comparatively good correlation of Ws with SP H_s ($R^2 = 0.47$; Fig. 6f). Because elevated SP H_s does

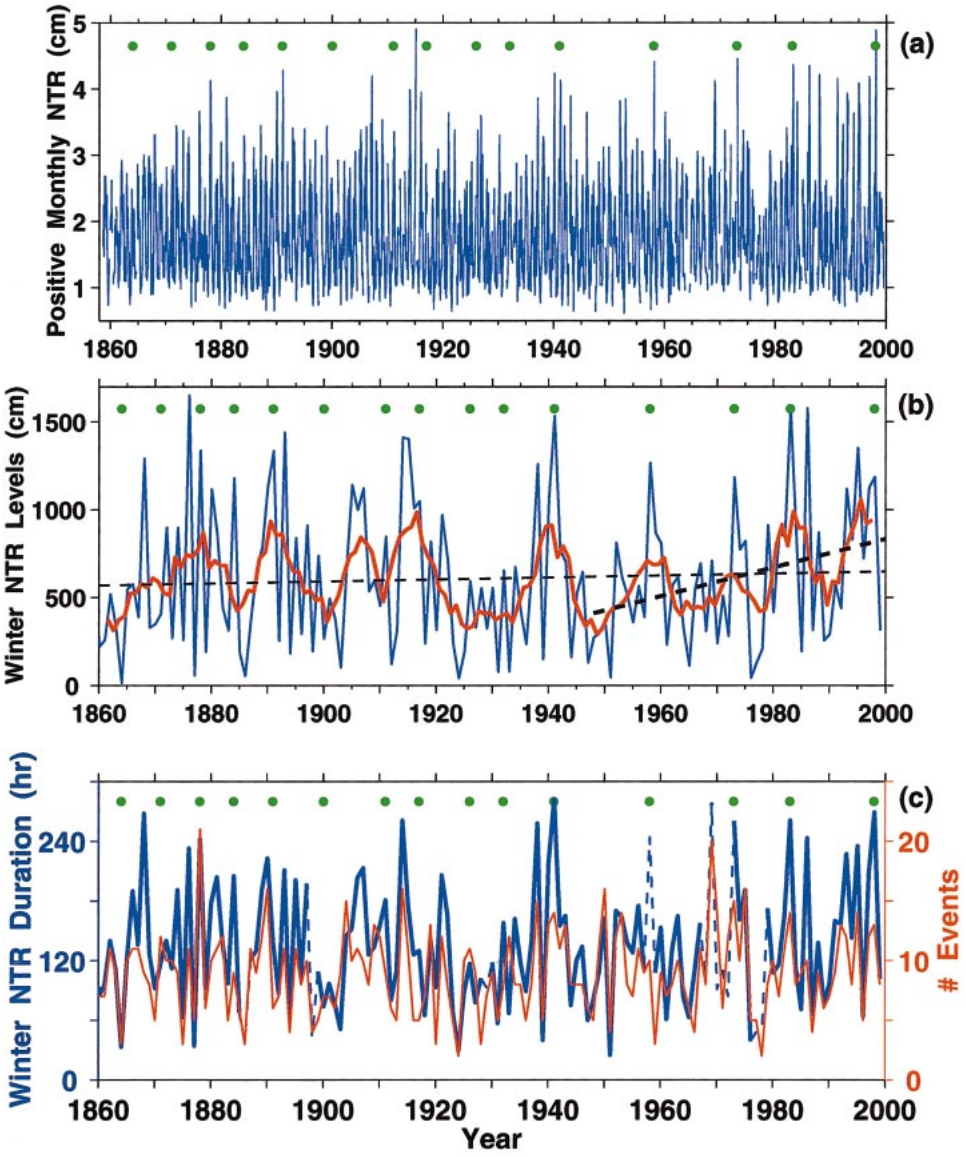

FIG. 7. (a) Mean monthly positive NTR water levels for the last 140 yr. (b) Cumulative extreme NTR (exceeding the 98th percentile level of 11.5 cm for the entire hourly NTR time series, see Fig. 5, dashed line) during winter months (Dec–Mar), with its 5-yr running mean (red line). Least squares trend estimates for the entire winter record and since 1948 (dashed lines). (c) Cumulative extreme winter hours (blue line) and events (red line). Dashed blue line indicates less than 90% of the hourly data were available, indicating that these periods may be underestimated. Times of strong, moderately strong, and very strong El Niños (Quinn and Neal 1987) are indicated by green dots (1998 was added).

occur under strong winds during storms, there is some correlation between SP H_s with NTRp (Fig. 6b) and SP H_s with SLP (Fig. 6d). All correlations in Fig. 6 are consistent with high NTRp being most closely associated with low SLP, that is, storminess. Similar correlations for summer months (June–September) are substantially reduced, with only correlations between NTRp and SLP ($R^2 = 0.33$) and between Ws and SP H_s ($R^2 = 0.11$) effectively different from zero. The observed relationship between NTRp and low SLP in Fig. 6a suggests that the variation of NTRp can be used as a proxy for regional storminess during winter months along the central California coast.

The monthly NTRp (Fig. 7a) indicate that elevated levels of storminess have occurred on numerous occasions over the past 140 yr, with high monthly NTRp levels often occurring during strong El Niños. Although the 1997/98 and 1982/83 El Niños produced high monthly NTRp at San Francisco, similarly high NTRp also occurred on several earlier occasions. However, not

all strong El Niño's coincide with high NTRp, and several high NTRp occurred in non–El Niño years (cf. green dots in Fig. 7a with NTRp levels). This observation appears to be in general agreement with studies suggesting that the North Pacific atmospheric response to warming in the tropical Pacific is modulated by the phase relationship between the warming and the North Pacific Oscillation (Gershunov and Barnett 1998). In any case, linear least squares analysis indicates no statistically significant long-term trend in monthly NTRp, suggesting that there has been no substantial change in storminess along the central California coast either for the last 140 yr or over the last 50 yr.

The variation of extreme NTR over winter months (December–March) provides an alternative comparison of North Pacific storminess variability. NTR levels above the hourly 98th percentile result from strong meteorological forcing, thus giving a measure of storms with high intensity (see Fig. 5; we note that the 2 percentile level for SLP at San Francisco 1948–99 is 1008.6 mb). Cumulative sums of NTR levels and the number of hours above the 98th percentile threshold for all hourly NTR give magnitude and duration measures, respectively, of extreme winter conditions. A single extreme event occurs for the time NTR persists above the hourly 98th percentile level. These cumulative indices (Figs. 7b and 7c) indicate that extreme storminess, compared with stormy winters prior to 1930, has not increased during recent El Niños. Note that some winters have extreme NTR levels nearly 10% of the time. Similar to monthly NTRp, not all strong El Niños coincide with high winter extreme NTR levels. There is a relatively small increasing trend in winter extreme NTR (0.56 cm yr^{-1}, thin dashed line, Fig. 7b), amounting to an increase of about 13% relative to the mean over the 140-yr record length. However, in contrast to monthly NTRp, there is a substantial increasing trend in winter extreme NTR levels since about 1950 (thick dashed line, Fig. 7b). This observation is consistent with similar increasing trends in winter sea surface temperature, zonal wind shear, and SLP observed over the North Pacific from 1948 onward (Graham and Diaz 2001). We note that the trends observed in these parameters by Graham and Diaz (and in winter extreme NTR levels) are strongly influenced by the limited record length available, in that, relative to 1948–78, there was heightened activity in the last two decades. Note that the extreme NTR data also indicate that this two-decade period was very active, but not extraordinarily so compared to pre-1948 epochs, for example, 1865–1915 (Fig. 7b), suggesting that it is unlikely that these increasing trends will persist. Interestingly, no comparable trends in either winter duration or the number of winter events (Fig. 7c) are observed.

Cumulative summer (June–September) NTR exceeding the 98th percentile level are nonzero for only 16 summers, with the summer extreme NTR maximum less than 10% of the mean of all winter extreme NTR. This underscores winter as being the dominant storm season in the midlatitudes of the eastern North Pacific, and reinforces the use of winter NTR as a measure of climatic changes in the region's storm activity.

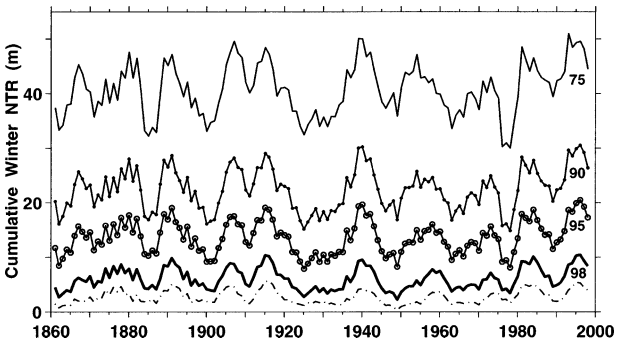

FIG. 8. The 5-yr running means of cumulative NTR exceeding the indicated percentile threshold levels. The 98th percentile threshold level for the bottom dashed line was determined from the ranking of hourly NTR estimates during only winter months (Dec–Mar), while thresholds for the upper four curves were determined from ranking the entire all-season hourly NTR time series. The all-data 98th percentile (thick solid line) curve is the same as in Fig. 7b (red line).

Sensitivity of the observed long period variability in NTR (Fig. 7b, red line) to the choice of the acceptance threshold is demonstrated in Fig. 8 for the 98th, 95th, 90th, and 75th percentiles determined from the ranking of all hourly NTR data. The threshold level decreases as the percentile level decreases, thus raising the cumulative winter NTR. Similarly, because restricting the 98th percentile level to ranking hourly data from just winter (December–March) months (dashed line) is about 25% higher than for the full-year (all data) 98th percentile level (thick solid line), the cumulative extreme NTR are lower. Only minor changes in the shape of the curves are observed with decreasing percentile and also for the December–March 98th percentile curve (broken line), indicating that the observed variability of NTR is not sensitive to the threshold selected. This strong resemblance of the winter NTR variability case (dashed line) to that of the all-season cases reflects the dominating influence of winter conditions in setting the tempo of California coastal storminess. The consistency of the variations across several threshold percentiles can be attributed to the relatively smoothly varying characteristics of SLP, the dominant NTR forcing. The 98th percentile level for the complete hourly dataset will be the reference level used in all following discussions of winter NTR.

Intense storm events cause the greatest coastal erosion and have the greatest impact on coastal structures. To investigate whether extreme storminess (as measured by winter NTR) has increased since 1860, running sums with 1-yr steps of winter NTR (blue line, Fig. 7b) and winter events (red line, Fig. 7c) were determined for scale lengths of 5, 10, 15, and 20 yr (Figs. 9a and 9b, respectively). The pattern of variability in Fig. 9 gen-

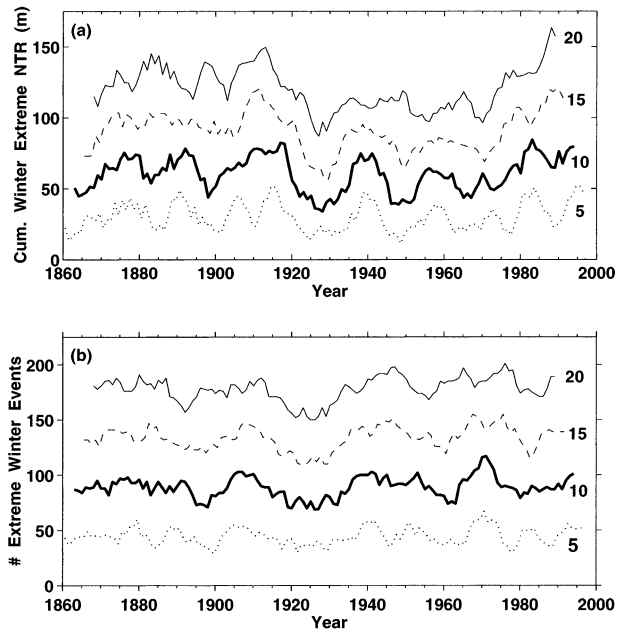

FIG. 9. Running sums of (a) winter NTR and (b) the number of extreme events exceeding the complete hourly 98th percentile threshold level during winter months (Dec–Mar). Sequential sums were computed with 1-yr steps for 5-, 10-, 15-, and 20-yr record lengths.

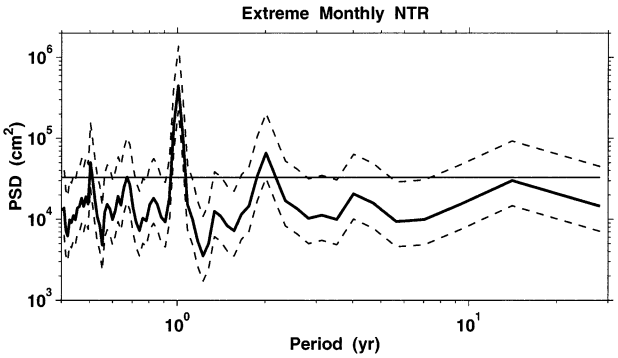

FIG. 10. Long-period variability from spectral estimates of cumulative monthly extreme NTR. Included are 95% confidence limits (dashed lines) and the 95% significance level (horizontal line).

erally follows the 5-yr running mean of winter NTR in Fig. 7b, with distinct increasing trends in cumulative NTR at all four timescales from about 1970 onward. In contrast, the cumulative number of events at these timescales have flat-to-decreasing trends during the post-1970 period. Thus, because fewer events generated higher cumulative NTR, this suggests that storm intensities have increased during the last three decades. However, as Fig. 5 shows, the number of events is clearly more sensitive to threshold level selection than cumulative NTR. Importantly, these curves all share similar fluctuations, indicating that the history of variability is not an effect of the filter structure. Neither measure of variability in Fig. 9 indicates any long-term trend in extreme storminess over the last 140 yr.

5. Interdecadal variability of extreme storminess

Many climate-related parameters have a red spectrum, that is, with energy generally increasing with increasing period but with no significant peaks in periodicity at periods longer than a few years (Wunsch 1992). Although no significant long-term trend in extreme storminess is observed in Figs. 7 and 8, the 5-yr running means do appear to exhibit some periodicity. The periodicity of extreme storminess variability was investigated by ensemble averaging power spectral density (PSD) estimates of the cumulative monthly NTR exceeding the 98th percentile level. The resulting monthly NTR time series was divided into five 28.2-yr records, each demeaned and detrended before application of a Hanning window and obtaining FFT PSD estimates. The resulting spectrum (Fig. 10) has spectral peaks near or above the 95% significance level at periods near 0.5, 1, 2, and 15 yr. These spectral peaks are consistently present for data record lengths varying from 70 to 20 yr (i.e., dividing the monthly NTR time series into two to seven segments), lending confidence that these peaks are not processing artifacts. The dominant peak at 1-yr periodicity shows the significance of the annual cycle, consistent with the dominance of winter storminess in determining the long-period pattern of extreme NTR variability demonstrated in Fig. 8. The significant peak near 2-yr and the minor peak near 4-yr periodicities seem to correspond to similar peaks observed in the November–March North Pacific index spectrum (Trenberth and Hurrel 1994). The spectral peak near 0.7 yr is not present at all record lengths, and therefore has less significance. The falloff in energy at periods above the 15-yr peak is consistent over all record lengths and in fact becomes more pronounced as the record length increases, suggesting that the spectrum of extreme storminess is not red and exhibits some interdecadal periodicity.

The multiyear pattern of storminess variability can also be characterized by 5-yr running means with 1-yr steps of winter extreme NTR. Winter NTR levels (Fig. 7b, red line) and winter NTR duration (Fig. 11a, solid line) suggest interdecadal quasiperiodicity, consistent with the spectral peak near the 15-yr period in Fig. 10. Elevated 5-yr means observed in the last 10 years coincide with persistent El Niño conditions in the equatorial Pacific in the early 1990s (Trenberth and Hoar 1996), and the strong 1997/98 El Niño. Post-1935, the peaks in the 5-yr mean winter NTR occur near recognized strong El Niños (Quinn and Neal 1987), reflecting the heightened North Pacific storm activity during El Niño episodes. The prominence of this peak is a confirmation of the effect of the well-known amplification of the winter Aleutian low system in the North Pacific during tropical Pacific warm episodes (Bjerknes 1969;

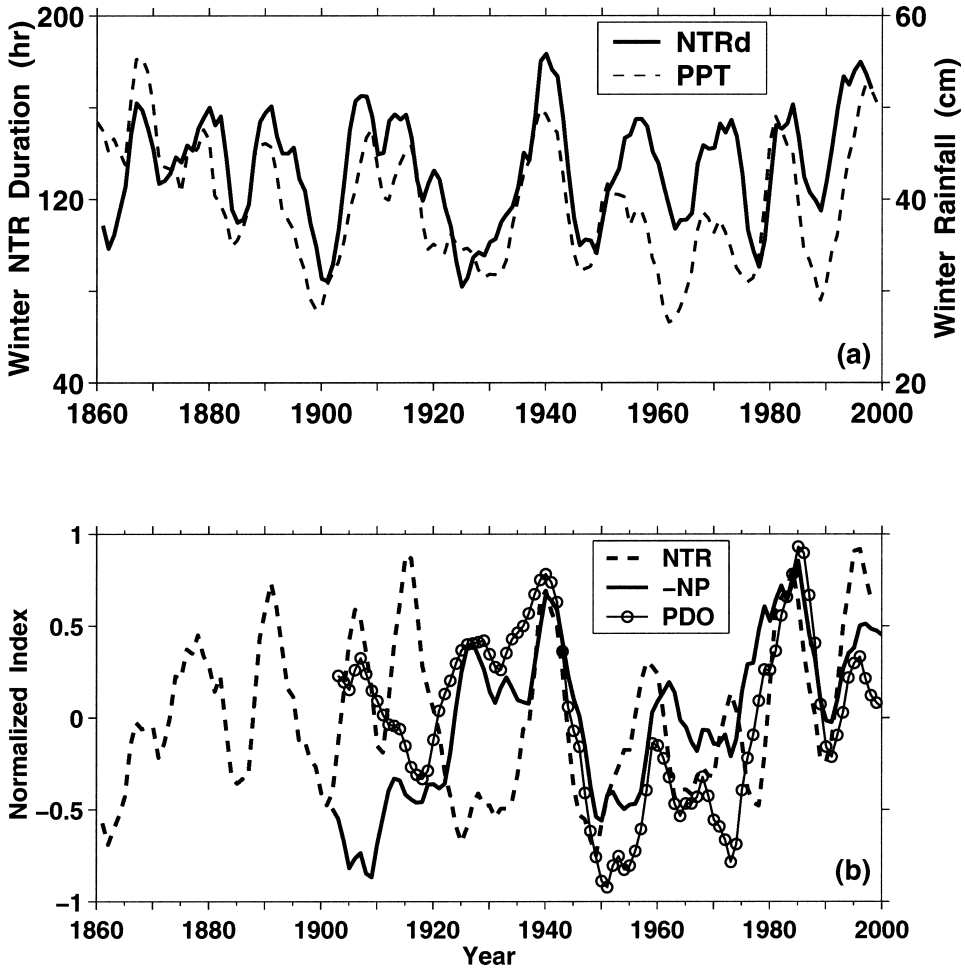

FIG. 11. (a) Running means (5-yr) of total winter hours that NTR exceeded the 98th percentile (NTRd, solid line, see Fig. 7c) and cumulative winter precipitation (PPT, dashed line) at San Francisco. Both show distinctive patterns of decadal-scale variability. The duration of extreme water levels at SFO has remained remarkably consistent during periods of heightened storm activity over the past 140 yr; (b) Normalized 5-yr running means of winter extreme NTR and the −NP and PDO indices. Note that −NP is plotted so that NP troughs correspond to high NTR episodes.

Mo and Livezey 1986; Graham 1994) in affecting weather patterns along the California coast over the last 60 yr.

The significance of interdecadal patterns of winter NTR variability can be assessed by comparison with other climate-related parameters. Running means were obtained for the cumulative winter (December–March) extreme duration NTR (NTRd) and the mean winter precipitation for successive 5-yr periods with 1-yr steps. Although some differences are observed, winter precipitation at San Francisco has peaks and troughs in the 5-yr running means (dashed line, Fig. 11a) near those of winter NTRd, with the pattern of precipitation variability even more closely matching that of winter NTR levels (Fig. 7b). This observation is born out by correlations between the normalized 5-yr running means of winter precipitation and winter NTR ($R^2 = 0.33$) and of precipitation and winter NTRd ($R^2 = 0.46$), with expected good correlation observed between NTR and NTRd ($R^2 = 0.70$). Similar patterns of interdecadal variability are also observed from 5-yr running means of North Pacific sea surface temperature, zonal wind shear, and SLP from 1948 onward (Graham and Diaz 2001). The consistency across these parameters suggests that the variation in winter NTR levels at SFO gives a reasonably good estimate of interdecadal storminess variability over the North Pacific.

During the post-1935 era, winter NTR variability corresponds reasonably well with the general pattern of the Pacific decadal oscillation (PDO; Mantua et al. 1997) and the North Pacific (NP) index (Trenberth and Hurrell 1994). Normalized 5-yr running means with 1-yr steps of winter (December–March) extreme NTR and winter NP and PDO indices (Fig. 11b) show that relatively low

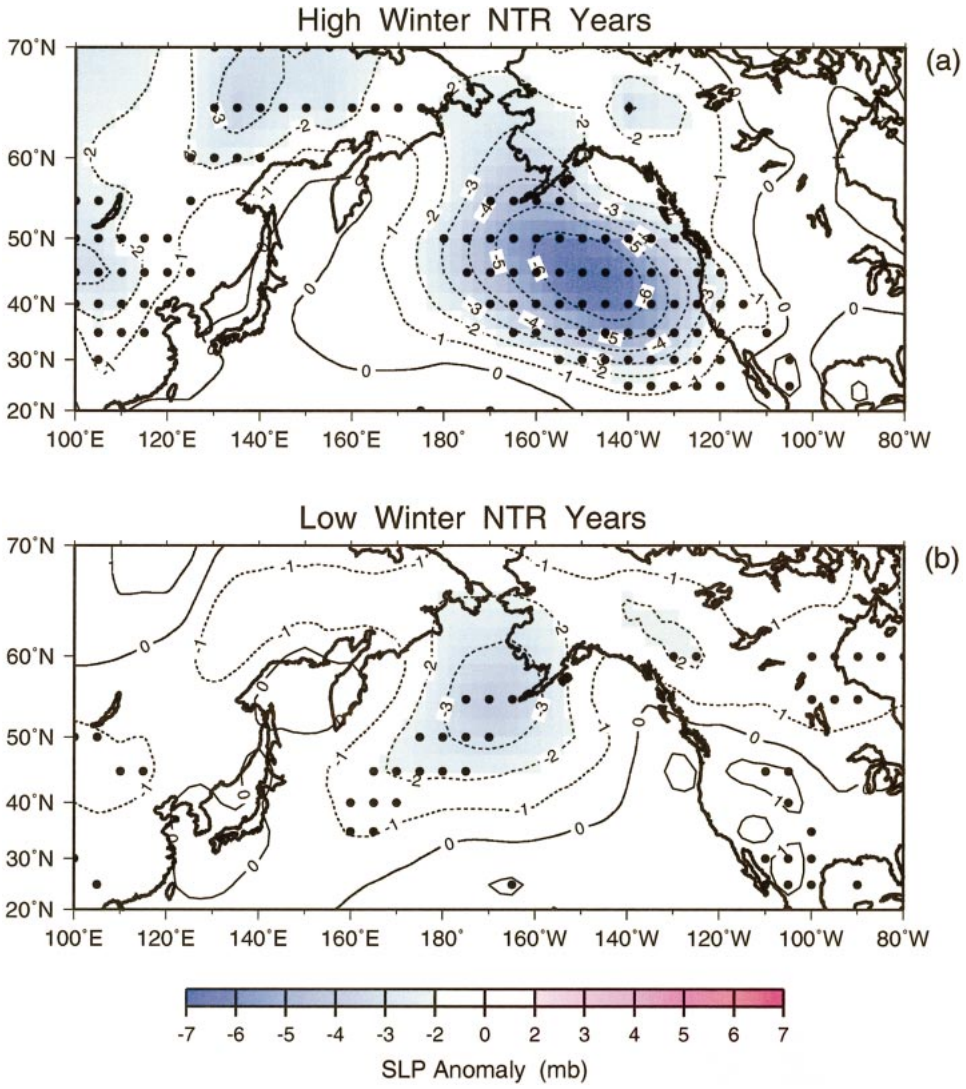

FIG. 12. Composites of winter (DJF) SLP anomalies for post-1900 extremes of (a) high and (b) low winter NTR. Winters included are the top ($n = 14$) and bottom ($n = 15$) 10% of winter extreme NTR in Fig. 7. Low pressure (dashed contours) and high pressure (solid contours) anomalies show the dominant extreme winter patterns. Grid locations whose composite anomaly is significantly different from the null hypothesis at ≥95% confidence are designated by dots.

storminess levels from the mid-1940s to the mid-1970s occurred during the cool phase of the PDO under relatively high mid-Pacific atmospheric pressure as indicated by the NP index. It should be noted that prior to 1935, the correspondence between the NP and PDO indices with NTR is not good (Fig. 11b). This suggests that a major change in North Pacific storm tracks may have occurred during the 1930s. Also note the divergence between the NP and PDO indices prior to about 1920, suggesting that other components of the climate system were not following the modern teleconnection pattern. Substantial shifts in North Pacific climate patterns and teleconnections have been noted in previous studies of ENSO (e.g., Hoerling and Kumar 1997; McCabe and Dettinger 1999; Gershunov and Barnett 1998). The SFO NTR-inferred storminess thus suggests both midlatitude and tropical associations to quasi-oscillatory interdecadal variability in the North Pacific, as described in previous studies (Latif and Barnett 1994; Miller and Schneider 2000).

Does the pattern in winter NTR variability at SFO have broad significance that extends to atmospheric variability across the North Pacific basin? To establish the relationship of storminess variability at SFO to broad-scale atmospheric circulation patterns, SLP anomaly composites were determined for years having exceptionally high and low winter NTR in Fig. 7b. These anomalies were mapped over a 5° latitude–longitude

Northern Hemisphere grid. The statistical significance of each location's composite anomaly was judged via a null hypothesis by gauging against the overall mean anomaly (zero) using a two-tailed *t* test. Two distinct SLP anomaly patterns emerge: (i) a broad region of highly significant negative anomalies across midlatitudes of the central and eastern North Pacific (high NTR, Fig. 12a), and (ii) a much weaker, more northerly Aleutian low (low NTR, Fig. 12b). The high NTR composite (Fig. 12a) features the intensified and southerly displaced Aleutian low that is characteristic of the Northern Hemisphere atmospheric circulation's response to El Niño (Bjerknes 1969; Namias 1976). The atmospheric pressure pattern in Fig. 12a is clearly much more likely to produce intense storminess both in the central North Pacific and along the West Coast. This negative pressure anomaly is stationed much farther east than the North Pacific low pattern associated with the NP index (Trenberth and Hurrell 1994), indicating the importance of the eastern North Pacific regime. The distinct contrast between composites associated with high versus low winter NTR demonstrates the strong influence of broad-scale North Pacific atmospheric circulation in driving storminess along the California coast, and alternatively, the utility of San Francisco NTR as an indicator of winter storminess over extensive regions of the North Pacific Ocean and western North America.

6. Implications for climate-related trends

Pronounced multiyear fluctuations of San Francisco winter sea level extreme nontidal residuals (Figs. 7b and 11) are prominent features of this long historical record, evidently reflecting pulsations in winter climate patterns across the North Pacific basin. Although heightened storminess has occurred during the last two decades, the activity levels observed are not exceptional compared to earlier periods such as the early 1900s and the late 1930s to early 1940s. The recent heightened storminess results in an increasing trend in extreme (high) sea level residuals over the last 50 years. Increasing trends in climate-related variables have also been identified by recent studies of cyclone frequency (Graham and Diaz 2001) and wave height (Allen and Komar 2000), also strongly influenced by similar heightened activity in the last two decades. Continuation of these increasing trends would have serious consequences for structures and ecosystems along the West Coast. However, recent activity seems to have peaked during the great El Niño event of 1997/98. If the observed historical pattern of interdecadal, quasi-cyclic winter storminess holds true, the heightened activity during the late 1990s should subside for the next decade or so.

Acknowledgments. The California Department of Boating and Waterways sponsored this study as part of its boating facilities and safety program. We thank Len Hickman of NOAA for copying and supplying the pre-1900 hourly tide data on paper and Tony Westerling of SIO for managing the digitizing process. We also thank Nick Graham for useful suggestions and Bob Guza at SIO for reviewing the manuscript. Special thanks to three anonymous reviewers and Editor Michael Mann for many excellent comments and suggestions that added substantially to the manuscript. D. Cayan was also supported by the NOAA Office of Global Programs Regional Integrated Sciences and Assessments (RISA) Program Element through the California Applications Program, by the U.S. Department of Energy Office of Science (BER), Grant No. DE-FG03-01ER63255, and by the U.S. Geological Survey Place-Based Studies Program on the San Francisco Bay/Delta.

REFERENCES

Allen, J., and P. Komar, 2000: Are ocean wave heights increasing in the eastern North Pacific? *Eos, Trans. Amer. Geophys. Union,* **81,** 561–567.

Anderson, J. R., and J. R. Gyakum, 1989: A diagnostic study of Pacific basin circulation regimes as determined from extratropical cyclone tracks. *Mon. Wea. Rev.,* **117,** 2672–2686.

Bjerknes, J., 1969: Atmospheric teleconnections from the tropical Pacific. *Mon. Wea. Rev.,* **97,** 163–172.

Cartwright, D. E., 1972: Secular changes in the oceanic tide at Brest, 1711–1936. *Geophys. J. Roy. Astron. Soc.,* **30,** 433–449.

Chelton, D. B., and R. E. Davis, 1982: Monthly mean sea-level variability along the west coast of North America. *J. Phys. Oceanogr.,* **12,** 757–784.

Enfield, D. B., and J. S. Allen, 1980: On the structure and dynamics of monthly mean sea level anomalies along the Pacific coast of North and South America. *J. Phys. Oceanogr.,* **10,** 557–578.

Flick, R. E., 1986: A review of conditions associated with high sea levels in Southern California. *Sci. Total. Environ.,* **55,** 251–259.

Gershunov, A., and T. P. Barnett, 1998: Interdecadal modulation of ENSO teleconnections. *Bull. Amer. Meteor. Soc.,* **79,** 2715–2725.

Graham, N. E., 1994: Decadal-scale climate variability in the tropical and North Pacific during the 1970s and 1980s: Observations and model results. *Climate Dyn.,* **10,** 135–162.

——, and H. F. Diaz, 2001: Evidence for intensification of North Pacific winter cyclones since 1948. *Bull. Amer. Meteor. Soc.,* **82,** 1869–1893.

Hoerling, M. P., and A. Kumar, 1997: Why do North American climate anomalies differ from one El Niño to another? *Geophys. Res. Lett.,* **24,** 1059–1062.

Krauss, T. P., L. Shure, and J. N. Little, 1995: *Signal Processing Toolbox User's Guide.* The Math Works, 363 pp.

Latif, M., and T. P. Barnett, 1994: On the causes of decadal climate variability over the North Pacific and North America. *Science,* **266,** 634–637.

——, and Coauthors, 1998: A review of the predictability and prediction of El Niño. *J. Geophys. Res.,* **103C,** 14 375–14 393.

Mantua, N. J., S. R. Hare, Y. Zhang, J. M. Wallace, and R. C. Francis, 1997: A Pacific interdecadal climate oscillation with impacts on salmon production. *Bull. Amer. Meteor. Soc.,* **78,** 1069–1079.

McCabe, G. J., and M. D. Dettinger, 1999: Decadal variations in the strength of ENSO teleconnections with precipitation in the western United States. *Int. J. Climatol.,* **19,** 1399–1410.

Miller, A. J., and N. Schneider, 2000: Interdecadal climate regime dynamics in the North Pacific Ocean: Theories, observations and ecosystem impacts. *Progress in Oceanography,* Vol. 47, Pergamon, 355–379.

Mo, K. C., and R. E. Livezey, 1986: Tropical–extratropical geopotential height teleconnections during the Northern Hemisphere winter. *Mon. Wea. Rev.,* **114,** 2488–2515.

Munk, W. H., and D. E. Cartwright, 1966: Tidal spectroscopy and prediction. *Philos. Trans. Roy. Soc. London,* **259A,** 533–581.
Namias, J., 1976: Some statistical and synoptic characteristics associated with El Niño. *J. Phys. Oceanogr.,* **6,** 130–138.
Pugh, D. T., 1987: *Tides, Surges and Mean Sea Level.* John Wiley and Sons, 472 pp.
Quinn, W. H., and V. T. Neal, 1987: El Niño occurrences over the past four and a half centuries. *J. Geophys. Res.,* **92C,** 14 449–14 461.
Reid, J. L., and A. W. Mantyla, 1976: The effect of the geostrophic flow upon coastal sea elevations in the northern North Pacific Ocean. *J. Geophys. Res.,* **81,** 3100–3110.
Smith, R. A., 1980: Golden Gate tidal measurements: 1854–1978. *J. Waterway, Port, Coastal Ocean Div., Proc. Amer. Soc. Civ. Eng.,* **106,** 407–410.
Trenberth, K. E., and J. W. Hurrell, 1994: Decadal atmosphere–ocean variations in the Pacific. *Climate Dyn.,* **9,** 303–319.
——, and T. J. Hoar, 1996: The 1990–1995 El Niño–Southern Oscillation event: Longest on record. *Geophys. Res. Lett.,* **23,** 57–60.
Wang, X. L., and V. R. Swail, 2001: Changes of extreme wave heights in Northern Hemisphere oceans and related atmospheric circulation regimes. *J. Climate,* **14,** 2204–2221.
Wunsch, C., 1992: Decade-to-century changes in the ocean circulation. *Oceanography,* **5,** 99–106.